Comparative assessment of the acoustic activity and the Pressure Stimulated Voltage in marble specimens under compression

Stavros K. Kourkoulis, Ermioni D. Pasiou
National Technical University of Athens, School of Applied Mathematical and Physical Sciences, Department of Mechanics, Zografou Campus, 5 Heroes of Polytechneion Avenue, 157 73, Attiki, Greece
stakkour@central.ntua.gr, http://orcid.org/0000-0003-3246-9308 (SKK)
epasiou@central.ntua.gr, https://orcid.org/0000-0003-1580-3415 (EDP)

Dimos Triantis, Ilias Stavrakas
University of West Attica, Department of Electrical & Electronics Engineering, Electronic Devices and Materials Laboratory, Ancient Olive Grove Campus, 250 Thivon Avenue, 122 44, Athens, Greece
triantis@uniwa.gr, http://orcid.org/0000-0003-4219-8687 (DT)
ilias@uniwa.gr, https://orcid.org/0000-0001-8484-8751 (IS)

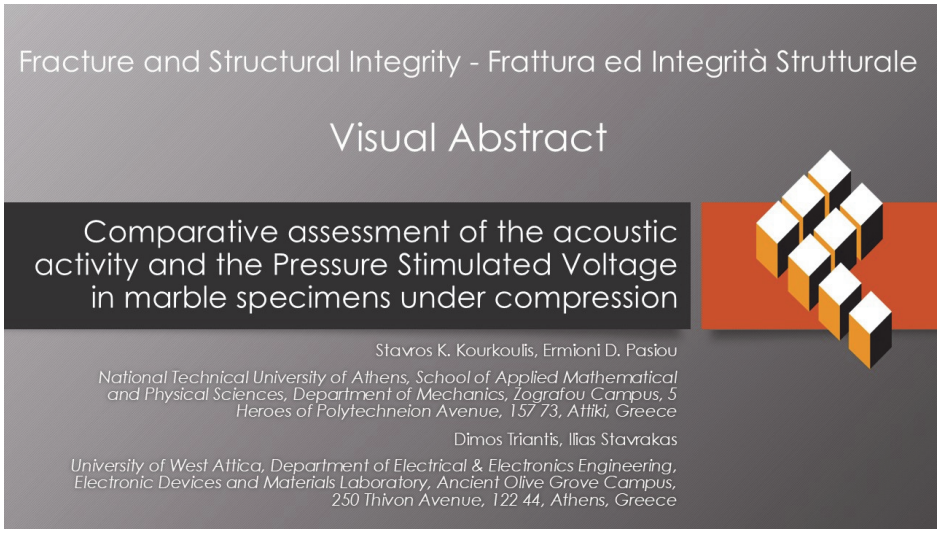

Citation: Kourkoulis, S.K., Pasiou E.D., Triantis D., Stavrakas I., Comparative assessment of the acoustic activity and the Pressure Stimulated Voltage in marble specimens under compression, Fracture and Structural Integrity, 72 (2025) 179-192.

Received: 23.01.2025
Accepted: 01.03.2025
Published: 03.03.2025
Issue: 04.2025

KEYWORDS. Pressure Stimulated Voltage; Acoustic Emissions; Pressure Stimulated Currents; F-function; Marble.

INTRODUCTION

Prediction of upcoming disastrous failures of engineering structures concerns the community of Structural Engineers from the dawn of civilization. Especially for the discipline of Earthquake Engineering, the detection of signals that could early warn about upcoming seismic events is equivalent to finding the Holy Grail. The respective research is continued uninterrupted and intensively long ago and this is, perhaps, the reason that most of the theories and techniques

related to the detection of pre-failure indices were firstly developed and applied in the direction of predicting upcoming strong earthquakes. Although, for the moment being, the specific target is not achieved, things are, at least, encouraging in the laboratory environment (which can be relatively easily "sterilized" from "external noises"): the techniques developed have indeed highlighted the existence of signals that can be considered as pre-failure indices. Among these techniques the one based on the detection and exploitation of Acoustic Emissions [1] is the most mature and successfully applied worldwide one for Structural Health Monitoring (SHM) purposes. The specific technique takes advantage of the mechanical waves generated within the bulk of a loaded system (either it is a specimen or a structural member or a structure or, even, the crust of the Earth) due to the sudden redistribution of local stress fields and the consequential abrupt release of elastic strain energy, caused, for example, by the generation of micro-cracks, or the activation of other damage mechanisms.

However, the process of micro-cracking is responsible for additional geophysical emissions, detected in the form of micro-seismic excitations [2], infrared radiation [3], electromagnetic radiation [4], and, also, electric emissions, quantified either in the form of Pressure Stimulated Currents (PSC) [5] or in the form of Pressure Stimulated Voltage (PSV) (sometimes denoted as Electric Potential, EP) [6]. The PSC and the PSV are due to the same damage mechanisms, which are analogous to the mechanisms responsible for seismic excitations. A variety of theories have been proposed to explain the mechanisms that are responsible for the generation of electric emissions. One could mention, indicatively only, the Moving Charged Dislocations (MCD) model [7], and the theory of outflow of positive holes [8].

Nowadays, interesting monitoring techniques have been developed based on both PSC and PSV, which are considered as flexible SHM tools, complementary to those based on the Acoustic Emissions. They have been successfully applied for the study of the mechanical response and the evolution of damage within specimens made of concrete [5, 9, 10], marble [4, 5, 11], granite [4, 12], sandstone [4, 13], coal [14, 15] and other rocks [16, 17]. The results of these studies converge to that the electric signals are of very low intensity and of smooth (or imperceptible) increase for load levels within the elastic region of the loaded material. They start increasing gradually, according to an accelerating manner, only after the load exceeds the threshold designating onset of thermodynamically irreversible deformations. As the load approaches its peak value the electric signals exhibit a global maximum. The specific response provides a series of signs that can be considered as safe pre-failure indices [5, 18-20]. Very good correlation between the outcomes of the Acoustic Emissions technique and the techniques based on electric emissions has been highlighted in a series of research papers, especially concerning the pre-failure indices detected by each technique [5, 6, 13, 14]. It is very interesting to emphasize that according to recent studies the indices provided by exploiting the electric signals precede slightly the ones provided by the acoustic activity [5, 21].

The potential correlation between AE and PSV (or, more generally, between acoustic and electric emissions) attracted the interest of the engineering community rather recently, and, as a result, the relative works are scarce. Indicatively only one could mention the pioneering study by Archer at al. [6] who definitely concluded that their "… *experiments demonstrate a very strong positive correlation between AE and PSV in both the non-quartzose halite and quartz rich granite* ..." specimens. In addition, they suggested that "… *the strong correlation between AE and PSV emissions provides good evidence that Electric Potential Signals could be used as a cost-effective complementary technology, and possibly even an alternative, to piezo transducers*" [6]. Along the same line Zhang et al. [13] concluded that "… *In different failure stages of sandstone specimens, the Electric Potential Signal shows a periodic change characteristic, which has a good corresponding relationship with AE counts* …". In addition, Zhang et al. [13] attempted to arrange in chronological order the pre-failure signals provided by the Acoustic Emissions and the Electric Potential Signals. They arrived to the conclusion that "… *Compared with the Electric Potential Signal time series, the precursory point of the AE count time series also appears during the accelerated damage development stage of sandstone samples, with a lag time of 7.3 s. In terms of monitoring and early warning, the Electric Potential precursory point has more advantages*" [13].

Within the frame of the above argumentation, the electric activity developed in marble specimens submitted to uniaxial compression, will be quantified in the present study in terms of the PSV recorded. The electric activity will be considered in juxtaposition to the respective acoustic one, which will be quantified in terms of the F-function [5], and, also, in terms of the energy content of the acoustic signals. The latter, i.e., the fact that the correlation between the acoustic activity and the respective electric one is attempted in quantitative terms using parameters with either temporal (F-function) or energy characteristics, is among the innovative aspects of the present study. Moreover, the temporal evolution of the PSV will be analyzed in juxtaposition to the respective one of the PSC filling a knowledge gap of the literature, since the intrinsic relation between these two different manifestations of the electric activity developed while loading brittle materials is not as yet properly highlighted. Another novel aspect of the study is that the potential influence of the loading rate on the correlation between the acoustic and electric activities is explored (although at a preliminary stage). Finally, following Zhang et al. [13] additional experimental evidence will be added on the time sequence of appearance of the pre-failure indices provided by the Acoustic Emissions and Electric Signals, in an attempt to further assess the potentialities of the Electric Signals (either quantified in terms of the PSV or the PSC) to be used as SHM tools, complementary to those based on Acoustic Emissions.

EXPERIMENTAL PROTOCOL: THE MATERIAL, THE SPECIMENS AND THE EXPERIMENTAL SET-UP

The specimens of the present experimental protocol were made of a fine white marble, quarried from mountain Dionysos in the Attiki region, Greece. Its main physico-mechanical properties are close to those of Pentelic marble, the building stone used by ancient Greeks for the erection of the Athenian Acropolis monuments. Due to this, Dionysos marble is used extensively to cover the needs of the ongoing restoration/conservation project of the monuments of the Acropolis of Athens, implemented by the "Acropolis Restoration Service" under the auspices of the "Committee for the Conservation of the Acropolis Monuments", an interdisciplinary committee of the Greek Ministry of Culture. To the best authors' knowledge there are not prior studies investigating the correlation between AE and PSV for this material.
Dionysos marble is an anisotropic rock. Its mechanical properties, as they are obtained from the relative literature, exhibit strong scattering. It could be mentioned characteristically that for its tensile strength the values reported vary in the interval from about 2.5 MPa to about 19.5 MPa. Similarly, for its modulus of elasticity experimental values ranging from 23 GPa to about 90 GPa have been reported [22]. The above scattering (besides the inherent variability of the mechanical response of rock-like materials, the mechanical properties of which depend strongly on the exact quarrying position and depth) is well attributed to the anisotropic nature of Dionysos marble, which is in fact an orthotropic material characterized by three distinct directions of anisotropy. Vardoulakis and Kourkoulis [23], after long series of uniaxial compression and direct tension tests, with specimens cut along the three anisotropy axes, concluded that the mechanical properties of Dionysos marble along the two of the above anisotropy directions are very similar to each other, as it can be seen in Tab. 1. Taking into account the data of Tab. 1, it is concluded that, in a first approximation, Dionysos marble could be modelled as a transversely isotropic material, with only two independent anisotropy directions.

Property → Direction↓	Modulus of Elasticity [GPa]	Poisson's ratio [---]	Tensile strength [MPa]	Compressive strength [MPa]
Strong	84.5	0.26	10.8	82.5
Intermediate	79.5	0.26	9.5	78.2
Weak	50.0	0.11	5.3	48.2

Table 1: Numerical values of some critical mechanical properties of Dionysos marble along the three characteristic anisotropy directions [23] as they were obtained from quasi-static experiments under displacement-controlled conditions (loading rate equal to 10^{-6} m/min).

In addition, Vardoulakis and Kourkoulis [23] pointed out that that the specific variety of rock material is bimodular: The modulus of elasticity under compression exceeds slightly that under tension. Another worth-mentioning feature of Dionysos marble is that it exhibits (according to a very pronounced manner) the size effect, namely the dependence of its mechanical properties on the size of the specimens used for the laboratory experiments. Especially for the Uniaxial Compressive Strength (UCS), this dependence is not monotonous but rather a global maximum appears for cylindrical specimens of length equal to about 125 mm (and length-to-diameter ratio equal to 2).
The specimens of the present experimental protocol were shaped in the form of orthogonal prisms. The dimensions of their cross section were equal to 40 mm x 40 mm, while their length (height) was equal to 90 mm. Attention was paid for the specimens of the same class to be cut from the same core, since (as it was already mentioned) the properties of rocks and rock-like materials depend, among others, on the exact quarry point and depth. Comparing the results concerning the mechanical properties of the material, as they were obtained from the present protocol, against those mentioned by Vardoulakis et al. [23], it appears that the specific cores were oriented along the weak anisotropy axis.
The compressive load was applied along the longitudinal axis of the specimens by means of a very stiff servo-hydraulic INSTRON SATEC loading frame of capacity 300 kN. A representative axial stress-axial strain plot, from a typical experiment is shown in Fig.1a. Slight discrepancies for the mechanical properties depicted in Fig.1a and those in Tab. 1 are attributed to the different loading mode (load- versus displacement-controlled) and, also, to the "shape effect" (recall that the specimens used in the protocol realized by Vardoulakis and Kourkoulis [23] were cylindrical while those used in the present protocol were shaped in the form of orthogonal prisms. It is seen from Fig.1a that the response of Dionysos marble is linear elastic for the major portion of the interval of the applied stresses. It is only for very low loading levels and, also, when the load approaches the Uniaxial Compressive Strength (UCS) that the response deviates from linearity. The initial deviation from linearity is attributed to bedding errors and, also, to a kind of stiffening due to elastic closure of pre-existing defects and pores [24]. The second one is attributed to the onset of generation of thermodynamically irreversible phenomena, correlated strongly to significant accumulation of internal damage. In general, the second nonlinear region starts at load levels ranging from about 85% to about 92% of the UCS (at least for the specimens of the present protocol).

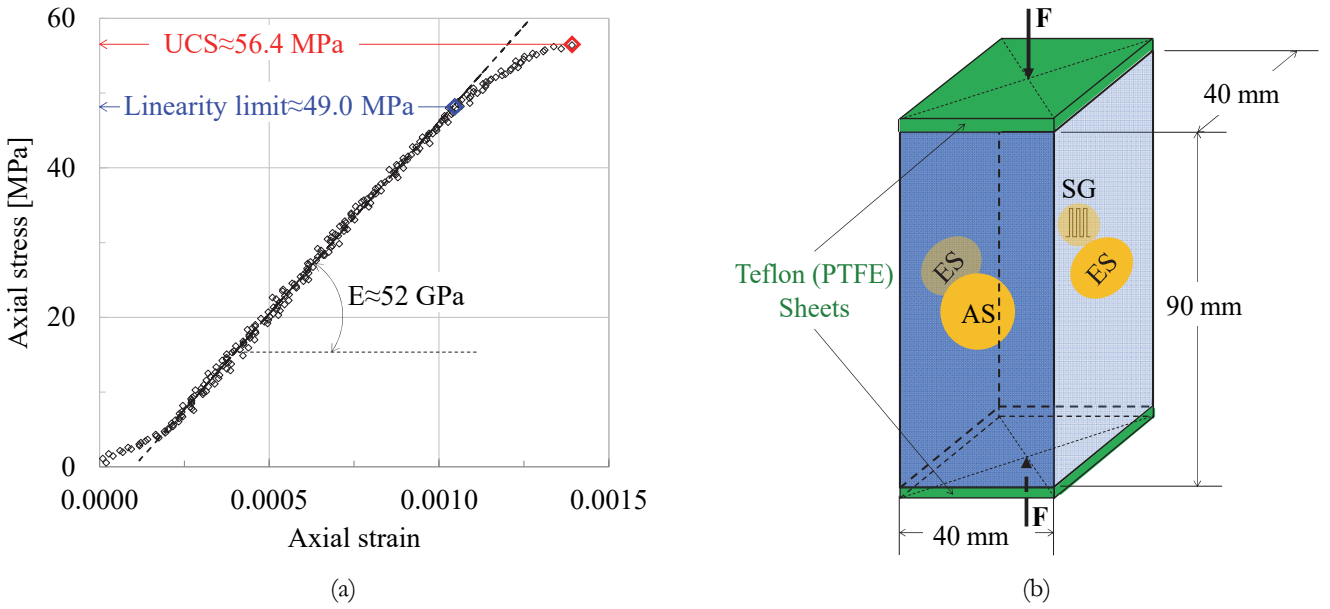

Figure 1: (a) A typical axial stress - axial strain plot of Dionysos marble under uniaxial compression. (b) Draft sketch of the specimens: The position of the acoustic sensor (AS), mounted on the center of the front lateral surface of the specimens, is depicted, together with the position of the two electrodes (electric sensors, ES), properly attached at the center of two opposite lateral surfaces and that of the electrical strain gauge SG, attached at the rear lateral surface.

The acoustic activity was recorded with the aid of an R6α acoustic sensor (mounted at the geometric center of the front lateral surface of the specimens, Fig.1b) with resonance frequency equal to 55 kHz and function bandwidth zone ranging in the interval from 35 kHz to 100 kHz. A preamplifier (gain 40 dB) was used, combined with analogue filters (pass zone in the range from 20 kHz to 400 kHz). The cut-off threshold was set to 40 dB. The equipment and software for detecting and recording the acoustic signals were provided by Mistras Group, Inc., Physical Acoustics Corp., New Jersey, USA. Given that only one sensor was used to capture the acoustic signals, it was deemed reasonable for the sensor to be placed as far as possible from the bases of the specimens in order to avoid recording signals due to friction effects between the loading platens and the bases of the specimens (although Teflon sheets were interposed between both bases of the specimens and the respective loading platens to minimize friction effects, see Fig.1b). In the direction of further reducing the role of any parasitic signals, proper timing parameters were selected regarding the AE system. This effort focuses mainly on the proper selection of parameters like the minimum inter-hit time (Hit Definition Time - HDT) and the attenuation factor of the specific variety of marble. These parameters were properly chosen after series of preliminary tests. In this context, when successive hits were recorded within time intervals approaching the time required for the AE to travel from the one side of the specimen to the other (matching the respective attenuation factor) it was straight forwardly concluded that the source of the specific signal is the same with that of the previous one and, thus, the specific signal is ignored as an outlier.

The respective electric activity, was quantified in terms of the PSV, using an ultra-sensitive electrometer (Keithley 6517A) of resolution equal to 1 fA and input impedance 200 TΩ using a pair of circular copper gold-plated electrodes that were attached at the geometric centers of two opposite lateral surfaces of the specimens. To achieve optimum electric contact, a thin layer of conductive silver paste was smeared at the points where the electrodes were to be attached. The backside of the electrodes was supported through additional thick Teflon sheets by springs that were used to keep the electrodes in position and ensure the uninterrupted contact during the loading process. Obviously, the Teflon sheets interposed to minimize friction effects (mentioned in previous paragraph) offer, also, electric insulation between the specimen and the loading platens. Finally, in order to assure that no electromagnetic noise distorted the recordings of the electric activity, the whole experimental set-up was placed in a Faraday cage. It is emphasized here that the background noise of the PSV signal recorded before the onset of the loading procedure was always lower than 0.1 mV for all the experiments of the present experimental protocol, without any exception at all.

Concerning the position of the electric sensor, it should be mentioned that it does influence the outcomes of any relative experiment, since the micro-fracturing processes responsible for the generation of the electric signals are not uniformly distributed all over the mass of the specimen. This was clearly highlighted by Stavrakas et al. [25], who used an integrated grid of five sensors (instead of a single pair of electrodes) to detect the electrical signals, that were emitted while submitting marble prisms to uniaxial compression. They clearly pointed out that the "… *use of such a grid of sensors does indeed enhance the*

capabilities of the PSC technique providing valuable information about the initiation and propagation of micro-fracturing at the interior of the specimens". In the present study the position of the single electric sensor used was decided taking into account that attention is focused to the comparative study of the acoustic and electric activities and, therefore, it was of critical importance for the two sensors (the electric and the acoustic one) to be placed as close to each other as possible. In addition, the specific position chosen (the central area of the specimen) limits possible effects of edge charges or any triboelectric or electrokinetic effects originating from the immediate vicinity of the loaded surfaces. In any case, it must be emphasized that the impact of the above-mentioned effects is rather negligible, since marble exhibits low porosity (non-electrokinetic), low quartz and high resistivity (non-triboelectric). Finally, it must be mentioned at this point that no cross-talking between the acoustic sensor and the electric voltage electrodes is possible and, therefore, placing them in the same position of the specimen has no impact on the measurements recorded.

The axial strains developed were recorded by means of an electric strain gauge attached at the specimens' rear lateral surface. Special attention was paid for the synchronization of all recording systems (i.e., the systems used to record the acoustic activity, the electric emissions, the axial strain and the applied load), an issue of extreme importance for proper interpretation of the experimental data [5, 26], which, if disregarded leads inevitably to erroneous results. In this direction, the PCI-2 (Mistras Group, Inc – Physical Acoustics Corp.) AE data acquisition card was used, equipped with parametric inputs, as it is analytically described in the user's manual of the manufacturer. These parametric inputs are used as an extra input to the AE system that can be used to measure any other external quantity from other transducers. In the present protocol the PCI-2 was used to capture the AE activity and the parametric data were used to record the mechanical load from the loading frame (which is equipped with analogue signal outputs that can be used to share the values of the load applied to other systems). Then, the numerical data for the load recorded were shared to all the measuring systems of the complete set-up. Regarding the AE recordings it is, also, noted that the software used to control the AE systems was the AEWin ® software (provided, also, by Mistras Group, Inc – Physical Acoustics Corp.). Parameterizing this software enables recording both hit driven and time driven data (in the specific protocol the AE hits including the corresponding load level as shared from the loading frame). Furthermore, and at an independent sampling rate of 0.1 s additional load values were recorded to ensure the ability to reconstruct the complete load curve from the AE system for accurate data synchronization. Concerning the synchronization of the PSV recording system, it was achieved using the shared load level from the loading frame. Specifically, the PSV and the axial strain recording subsystem includes a data acquisition card (National Instruments Corp. ® 16 bit data acquisition PCI card module) an analogue input of which is dedicated to the load proportional voltage output of the loading frame. The data are recorded in the same environment prepared using the Agilent Vee ® software for visualization and data storing. Considering the above-mentioned precautions and measures taken, it is safely stated that all recording systems employed in the present protocol were properly synchronized.

The specimens were submitted to uniaxial compression, adopting a load-controlled scheme. In an attempt to take into account, also, the potential influence of the loading rate on the correlation between the electric and the acoustic activities, two classes of experiments were implemented, one with loading rate equal to 34 kPa/s and a second one with loading rate equal to 140 kPa/s. Unfortunately, there is not a standard dictating numerical values for the specific parameter, and, also, there is a lack of relative studies in the literature. It could be anticipated at this point that the choice of these two loading rates is more or less an arbitrary decision of the authors. Indeed, this is the case, since an exhaustive analysis of the role of this parameter was not the core target of the present study. This is just a first approach towards the specific issue, and, in this context, a very low loading rate was chosen (approaching quasi-static conditions) together with a relatively higher one (almost four times higher), which, however, is by no means considered as an actual dynamic loading scheme. The loading rate was kept constant throughout the duration of the experiments of each class. The load was applied monotonically from the onset of the tests until the final macroscopic distraction of the specimens. Three specimens were tested for each class. The scattering of the results between the three specimens of each class was relatively low, concerning both the mechanical response and, also, the parameters of the electric and acoustic activities.

EXPERIMENTAL RESULTS

Criticality by means of the electric activity quantified in terms of the Pressure Stimulated Voltage (PSV) (Electric Potential - EP)

In this section the results obtained from two representative experiments (one from each class of specimens) are analyzed. For the first one, in which the specimen was loaded at a constant rate of 34 kPa/s, the fracture stress (or, equivalently, the Uniaxial Compressive Strength, UCS) was equal to about 56.3 MPa. In Fig.2 the temporal evolution of the PSV is plotted, in juxtaposition to that of the applied axial stress (the latter is, obviously, a perfectly linear segment given that load-controlled conditions were adopted). The sampling rate for the PSV was set equal to 1 sample/s, while the

background level of the respective signal before the onset of the loading procedure was equal to about 90 μV. It was deemed necessary to subtract this background level from the values of the PSV, and, therefore the data plotted in Fig.2 correspond to the "net" PSV developed during loading.

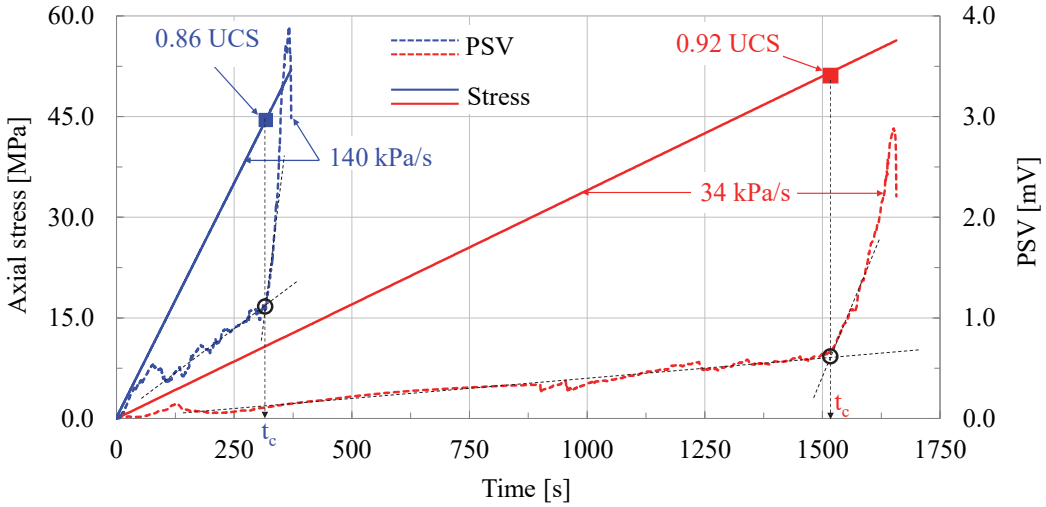

Figure 2: The temporal evolution of the "net" PSV and that of the applied axial stress for two characteristic experiments, one from each class of specimens tested (red lines and lettering correspond to loading rate equal to 34 kPa/s, while blue ones to 140 kPa/s.

It is observed from Fig.2 that the "net" PSV starts increasing abruptly at the time instant $t_c \approx 1520$ s, at which the respective axial stress applied is equal to about 92% of the respective peak level attained. Recalling that the stress level at which Dionysos marble ceases responding elastically (i.e., the limit after which the deformations become "permanent" or, equivalently, thermodynamically irreversible) was determined in the interval between 85% and 92% of the UCS, it could be concluded that the PSV starts increasing abruptly as soon as the material enters into its stage of non-reversible deformations. About 5.5 s before fracture the PSV attains a global peak, which for the specific experiment is equal to about 2.86 mV, and, then, it starts decreasing quite rapidly. The above-described response for the temporal evolution of the PSV is quite similar to the respective one of the PSC recorded in a series of experimental protocols with various loading schemes and specimens of various geometries made of a large variety of materials [5, 11, 12, 20, 27].

For the second experiment, the specimen was loaded at a constant rate equal to 140 kPa/s. The UCS was slightly lower from that of the previous experiment, and it was equal to about 52 MPa. This is, perhaps, unexpected, taking into account that, in general, increased loading rate corresponds to increased peak stress. Indeed, as it is mentioned by Rae et al. [28] "… *in general, results of mechanical testing demonstrate dynamic strength increase under uniaxial compression at large strain rates*". The specific inconsistency is clearly attributed to the fact that the two loading rates used in the present protocol are relatively close to each other, and, also, to the fact that the specimens of the two classes were cut from different cores.

The temporal evolution of the PSV and that of the axial stress applied, are plotted, also, in Fig.2, so that a direct comparison between the two classes of specimens to be clear. The sampling rate was again 1 sample/s. The background level of the electric signal, before starting the loading procedure, was equal to 65 μV and it was, again, subtracted from the values plotted in Fig.2. From a quantitative point of view the overall response of this specimen is similar to that of the previous one. There are, obviously, some quantitative differences: The PSV starts increasing abruptly at the instant $t_c \approx 317$ s, an instant at which the respective axial stress is equal to about 86% of the UCS. It seems, therefore, that the increased loading rate triggers the mechanisms responsible for the electric emissions at lower stress levels with respect to the loading at lower rate. Similarly to the previous specimen, 4.7 s before macroscopic fracture the PSV exhibits a global peak (higher than that of the lower loading rate) equal to about 3.9 mV.

In order to achieve a direct comparison of the electric activity generated in the two specimens, the "net" PSV recorded is plotted in Fig.3 for both experiments, versus the normalized time. The normalization is realized over the time instant of fracture, t_f, of each specimen, so that the horizontal axis of the two graphs to be common for the two specimens (i.e., $0<t/t_f<1$). Both the similarities and the differences between the two classes of specimens are now clearly highlighted: The PSV signal is almost linearly increasing for both specimens until the respective critical instants t_c, after which it starts increasing according to an explosive manner. A few seconds before fracture the signal exhibits a quite abrupt drop. For the specimen loaded at higher rate the PSV exceeds systematically that of the specimen loaded at lower rate for the overall duration of the experiments.

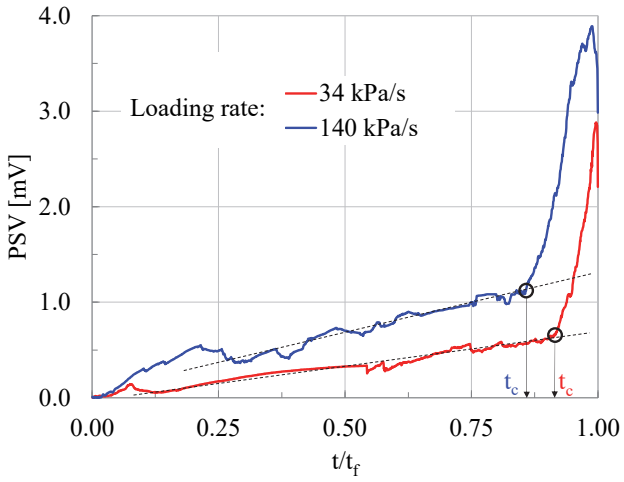

Figure 3: The "net" PSV recorded during each experiment (red lines and lettering correspond to loading rate equal to 34 kPa/s while blue ones to 140 kPa/s) versus the normalized (over the time instant of fracture, t_f, of each specimen) time.

Criticality by means of the acoustic activity quantified in terms of the F-function

The energy content of the acoustic hits, recorded from the onset of each experiment up to the fracture instant, are plotted in Fig.4 in juxtaposition to the axial stress applied, for both specimens analyzed (using the above adopted colouring code). There is not a striking difference between the number of acoustic hits recorded during the two experiments: they were equal to N_{34}=1079 for the loading rate of 34 kPa/s and N_{140}=1012 for the loading rate of 140 kPa/s. The main difference between the two experiments is that for the specimen loaded under higher rate significantly more acoustic hits are recorded during the early loading stages. It is mentioned, indicatively, that for the specimen loaded at 34 kPa/s only 2% of the overall number of acoustic hits was recorded up to a stress level equal to 50% of the UCS (light green rectangle in Fig.4a). The respective ratio for the specimen of the class with loading rate equal to 140 kPa/s approaches 15%.

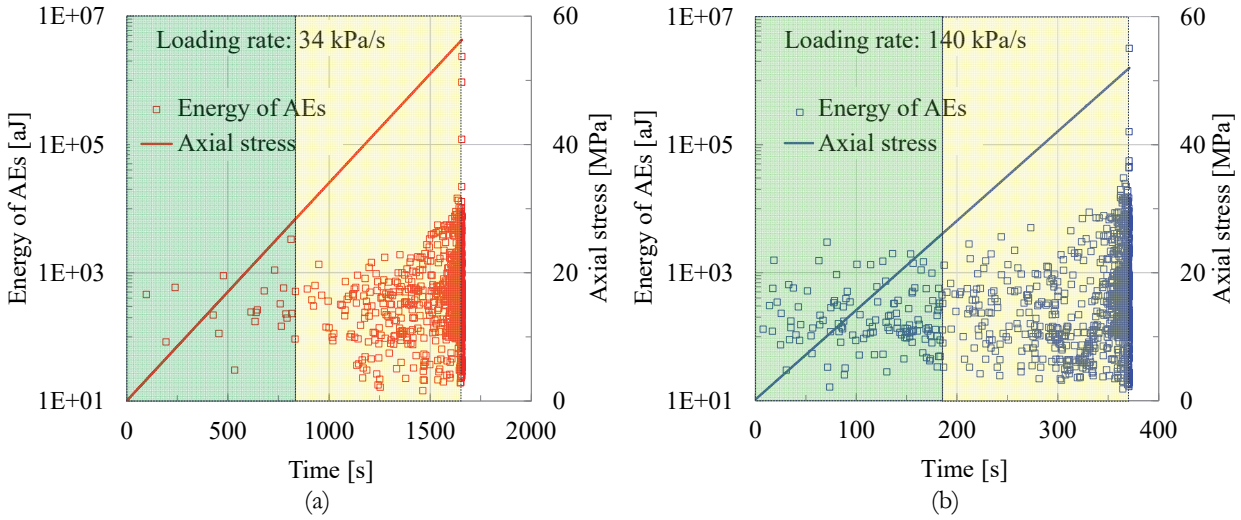

Figure 4: Temporal evolution of the energy content of the acoustic hits, recorded from the onset of each experiment up to fracture, for loading rate equal to (a) 34 kPa/s and (b) 140 kPa/s. Green rectangles correspond to $\sigma<(UCS/2)$ while yellow ones to $\sigma>(UCS)/2$.

In order, now, to describe quantitatively the intensity of the acoustic activity during the loading procedure, advantage is taken of the temporal evolution of the respective F-function, which represents the average frequency of generation of acoustic signals, within a given "window" of n successive signals [5]. The F-function is calculated as the "sliding" average of the instantaneous values $f_i=1/(\delta t_i)$ of the inverse interevent time intervals, (δt_i), between any two successive acoustic signals. The procedure for the determination of the F-function starts by considering a first "window" of acoustic signals, which includes the first n signals, where n is a relatively small fraction of the overall number N of the signals recorded. Although n is more or less arbitrarily chosen, its influence on the final conclusions is rather insignificant as long as n is small with respect to N. Further details about the role of n can be found in ref. [5]. For this first "window", one determines the

(n-1) interevent time intervals (δt_i) and the respective f_i-values. The mean value of these (n-1) f_i-values corresponds to the first value F_1 of the F-function. "Sliding" then the first "window" by one signal (i.e., considering the "window" including the signals from the 2nd one up to the (n+1)th one) the second value F_2 of the F-function is obtained and so on (concerning the "sliding" step, its value is defined taking into account the total number of acoustic signals recorded, and, also, the level of resolution that is to be achieved). For the temporal evolution of the F-function to be plotted, each F-value is paired to the respective "average time", τ, which is calculated as the mean value of the instants, t_i, at which each one of the signals of the specific "window" was recorded. The main advantage of the description of the acoustic activity in terms of the F-function is that it provides very fine "resolution", which is of crucial importance, especially during the very last loading stage (i.e., as the load approaches its peak value), since the number of signals recorded during this stage increases dramatically.
It has been verified that an abrupt increasing trend characterizes the temporal evolution of the F-function a few seconds before the final fracture. Series of experimental studies have proven that the onset of this abrupt increase of the numerical values of the F-function is a flexible (and safe) pre-failure index, early warning about entrance of the mechanically loaded system (the specimen in this study) into its critical stage, namely the stage of impending macroscopic fracture [5].
For the experimental protocol of the present study, the number of the signals of each "window" was set equal to n=30. The temporal evolution of the F-functions determined for the two experiments analyzed in previous sections is plotted against the "average time" parameter τ (adopting logarithmic scale for the F-function) in Fig.5a for the specimen loaded at a rate of 34 kPa/s and in Fig.5b for the specimen loaded at a rate of 140 kPa/s. The acoustic activity in the specimen loaded under higher rate appears much more intense. Such a response could be expected taking into account that almost the same number of hits (with respect to the number of hits recorded in the experiment loaded under low rate) was recorded in a much shorter time interval. For both experiments the F-functions exhibit quite abrupt increase tendency, as the load approaches the respective peak value. The onset of this abrupt increase is detected at a stress level equal to about 94% of the UCS for the specimens loaded under low rate. The respective ratio for the specimen loaded under high rate is equal to about 88% of the respective UCS. It is recalled that the onset of abrupt increase of the PSV was detected at ratios equal to 92% and 86% of the UCS, respectively. It can be, therefore, concluded that the agreement between the critical time instants (rapid increase of either the acoustic or the electric activities) as obtained from the temporal evolution of the PSV and that of the F-function is quite satisfactory, at least for the material tested in this protocol.

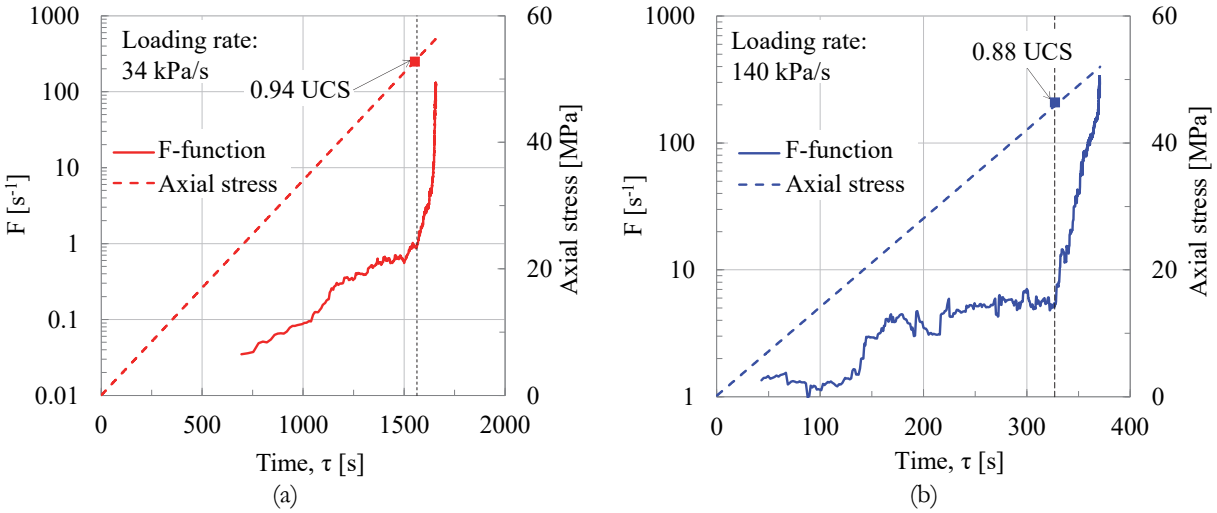

Figure 5: The temporal evolution of the F-function for the two representative experiments analyzed in this study plotted versus the "average time" parameter τ, along a semi-logarithmic system of axes (the values of the F-functions are plotted along a logarithmic scale). (a) Loading rate equal to 34 kPa/s; (b) Loading rate equal to 140 kPa/s.

To highlight further, comparatively, the temporal evolution of the acoustic activity generated during the two representative experiments discussed, the respective F-functions are plotted, in juxtaposition to each other, in Fig.6 versus a common axis, i.e., the normalized "average time" parameter, τ/t_f, where the normalization is implemented over the duration of each experiment. The huge quantitative differences between the two F-functions and, also, their qualitative similarities, are vividly seen: Both F-functions increase smoothly and almost linearly for the major portion of the loading process. As the load approaches its peak, the two F-functions exhibit an abrupt increasing trend. Moreover, it is observed that the acoustic activity in the specimen loaded under higher rate is systematically stronger, with respect to the one loaded under lower rate, for the overall duration of the experiments. A few seconds before fracture the signal drops abruptly for both specimens.

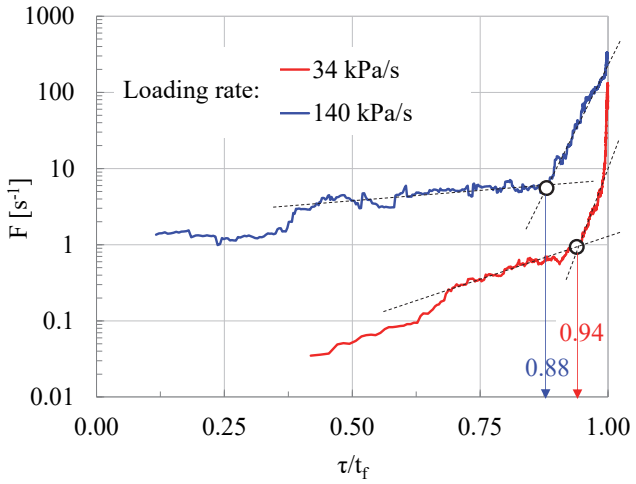

Figure 6: The F-functions of the two representative experiments discussed, plotted in juxtaposition to each other along a logarithmic scale, versus the normalized (over the duration of each experiment) "average time" parameter, τ/t_f.

Criticality by means of the acoustic activity in terms of the Cumulative Energy of the Acoustic Emissions

An additional Acoustic Emissions parameter, which is quite often used in the direction of detecting signs warning about impending approach of the loaded system (specimen) to the stage of accelerated damage processes (which will lead to the catastrophic fracture), is the Cumulative Energy of the Acoustic Emissions $(CE)_{AE}$. An abrupt increase of the temporal rate of the $(CE)_{AE}$ is usually conceived as a pre-failure index designating entrance into the stage of impending failure [29].

The temporal evolution of the $(CE)_{AE}$ for the two experiments analyzed here are plotted in Fig.7a, in juxtaposition to each other, in terms of the normalized (over the duration of each test) time. Attention is paid to the time interval $t/t_f > 0.7$, i.e., after a significant amount of acoustic energy is accumulated in the specimens. In Fig.7a the Cumulative Energies are plotted along logarithmic scale. It is observed from this figure that during the early loading steps (i.e., while the response of the specimens' material is still linear) the $(CE)_{AE}$ increases obeying, for both specimens, a power law of the following form:

$$(CE)_{AE} = \beta\left(\frac{t}{t_f}\right)^{\mu} \tag{1}$$

In Eq.(1) β is an energy constant and μ is an exponent related mainly to the level of the cumulative energy of the Acoustic Emissions of each test and the respective background level of the cumulative energy at lower stress levels. It is seen from Fig.7 that for the specimen loaded at high rate the values of the $(CE)_{AE}$ are systematically higher. This is well attributed to the

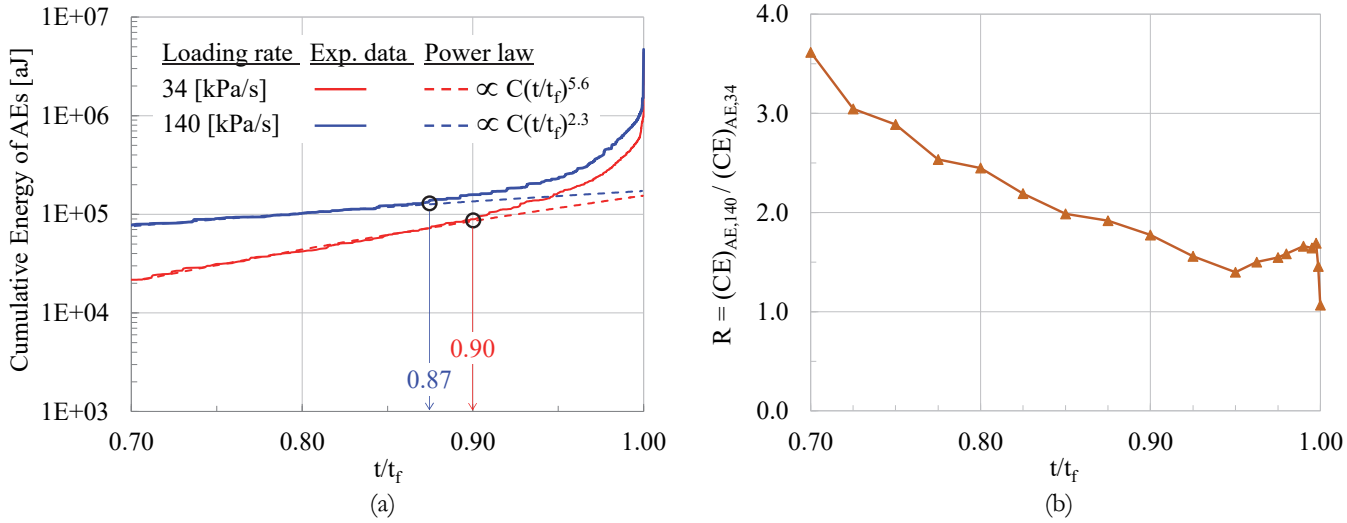

Figure 7: (a) The Cumulative Energy of the Acoustic Emissions, $(CE)_{AE}$, plotted in juxtaposition to each other along a logarithmic scale, versus the normalized (over the duration of each experiment) "average time" parameter, t/t_f. (b) The ratio of the two $(CE)_{AE}$.

fact that for this specimen an increased number of acoustic hits had been recorded during the early load levels, in accordance to the conclusions drawn from the temporal evolution of the rate of generation of the acoustic signals in terms of the F-function (see Fig. 6). In this context, the exponent μ is equal to μ=2.3 for the specimen with loading rate of 140 kPa/s while for that with loading rate equal to 34 kPa/s the exponent μ is equal to μ=5.6.
The above exponential law (Eq.(1)) governs the temporal evolution of the $(CE)_{AE}$ until the critical (normalized) instants $t/t_{f,34}=0.90$ and $t/t_{f,140}=0.87$, for the specimen loaded under low and high strain rates, respectively. From these instants on, the temporal rate of the $(CE)_{AE}$ increases more abruptly, according to an accelerating manner, until the instant of fracture. At this point, it is quite interesting to note that as the applied load tends to its peak value (i.e., while $t/t_f \rightarrow 1$), the difference between the two $(CE)_{AE}$ decreases. This is clearly seen in Fig.7b, in which the ratio, R, of the two $(CE)_{AE}$, namely, the ratio $R=[(CE)_{AE,140\ kPa/s}/(CE)_{AE,34\ kPa/s}]$ is plotted versus the normalized time, t/t_f, for the interval $0.70<t/t_f=1$.

Discussion

The underlying target of the present study was the detection of potential pre-failure indices, the existence of which would further support the use of the electric activity as a Structural Health Monitoring parameter, complementary to the respective ones provided by the Acoustic Emissions technique. In this direction, the electric signals that were emitted while Dionysos marble specimens were submitted to uniaxial compression were analyzed in juxtaposition to the respective Acoustic Emissions. The electric activity was quantified in terms of the Pressure Stimulated Voltage (PSV) (denoted, also, as the Electric Potential (EP)) that was detected with the aid of an ultra-sensitive electrometer. The results of the comparative analysis of the two activities highlight that both the PSV and the AEs can be considered as valuable and flexible complementary tools for Structural Health Monitoring purposes, since they provide quantitative information about the proximity of the loaded structure to its critical stage. The most intriguing common characteristic of the electric and acoustic activities is that the temporal evolution of the PSV and that of the rate of generation of acoustic signals (and, also, that of the Cumulative Energy of the Acoustic Emissions) exhibit a clearly distinguishable change of their increasing rate: Indeed, as the load exceeds the limit beyond which irreversible deformations are generated within the bulk of the loaded structure, an abrupt increasing trend is observed.
The stress level (normalized over the respective UCS), at which the above-mentioned abrupt changes are detected for each one of the parameters considered previously are shown in next Fig.8 for the two experiments analyzed in this study. The parameters considered in Fig.8 are the PSV, the F-function, and, the Cumulative Energy of the Acoustic Emissions $(CE)_{AE}$.

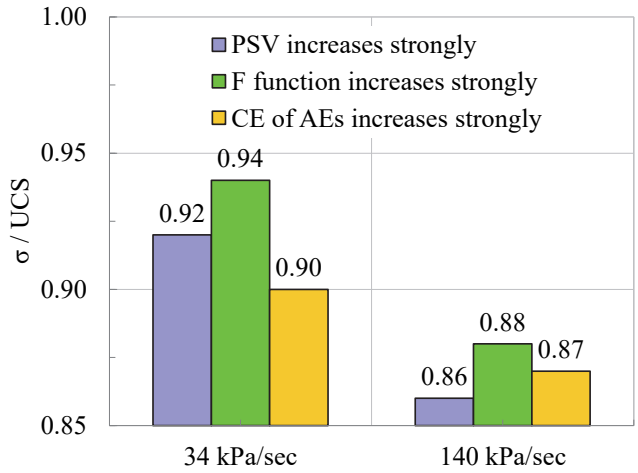

Figure 8: The normalized (over the respective UCS) stress at which the PSV, the F-function, and the Cumulative Energy of the Acoustic Emissions $(CE)_{AE}$ exhibit the abrupt change (abrupt increasing trend) of their temporal evolution, for the two loading rates studied.

It is clear from this figure that for the specimens loaded at higher rate the abrupt change of the temporal evolution of the acoustic and electric activities is observed at a lower stress level, independently of the parameter used. This stress level ranges in a very narrow interval, i.e., $0.86\leq\sigma/(UCS)<0.88$ for all three parameters (i.e., the PSV, the F-function and the $(CE)_{AE}$). The respective stress interval (at which the abrupt changes are detected) for the specimen loaded at low loading rate is $0.90\leq\sigma/UCS<0.94$. It is thus concluded, either considering the electric or the acoustic activity, that for increased loading rate the critical damage mechanisms are activated at earlier load levels.

Taking now into account that for Dionysos marble this is the first time that the electric activity is quantified in terms of the PSV, it was deemed interesting to comparatively consider the PSV against the respective Pressure Stimulated Current (PSC), which have been extensively studied in the past for Dionysos marble specimens under various loading schemes [5, 11, 12, 20, 21]. In this direction, an experiment is considered during which a specimen (of identical geometry to that of the specimens studied in previous paragraphs), is loaded under uniaxial compression and load-controlled conditions. An intermediate loading rate (compared to the rates adopted for the PSV), equal to 90 kPa/s is imposed. The UCS for the specific specimen was equal to 57 MPa. The temporal evolution of the PSC is plotted in Fig.9a in juxtaposition to that of the applied load. It is seen that up to the time instant $t_c \approx 567$ s (corresponding to a stress level equal to about 88% of the respective UCS), the PSC increases very slowly, according to an almost linear manner. From this instant on, the PSC increases quite rapidly towards a global maximum value equal to about 70 pA. A few seconds before the macroscopic fracture the PSC decreases rapidly.

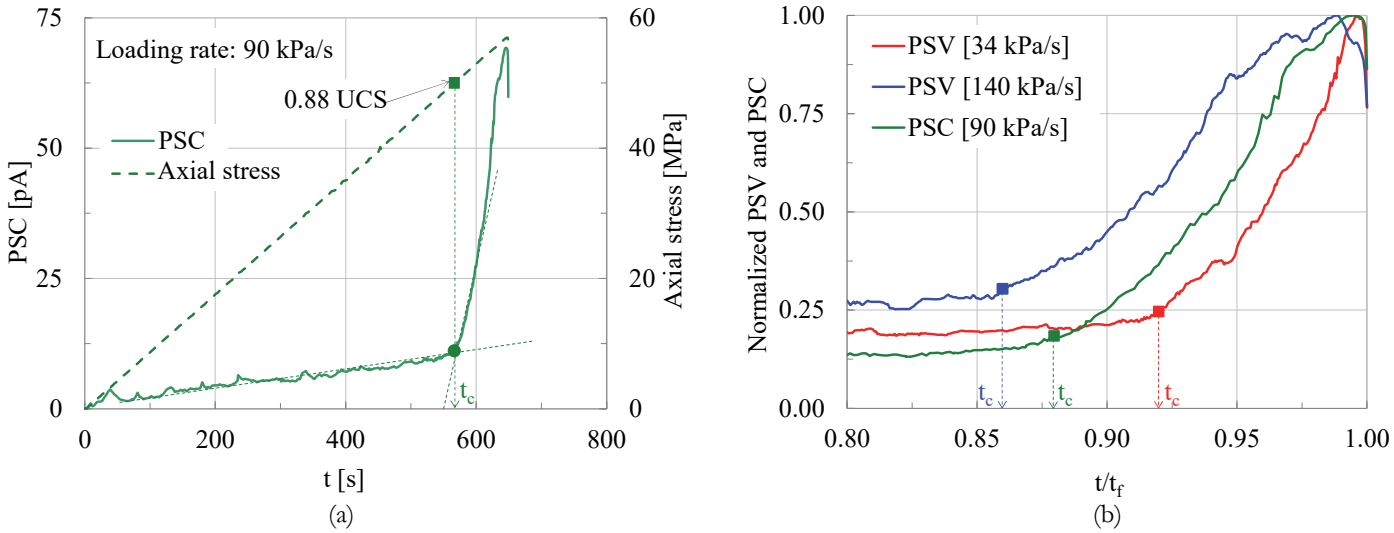

Figure 9: (a) The temporal evolution of the PSC and that of the applied load; (b) The evolution of the PSC in juxtaposition to the respective one of the PSV (for the specimens of the previous paragraphs) versus the normalized (over the fracture instant) time. Both the PSC and the PSV are normalized over the respective peak values attained.

In order now to highlight the similarities between the PSV and the PSC, their normalized (over the respective peak values) numerical values are plotted in Fig.9b versus the normalized (over the fracture instant, t_f) time, for the interval $0.80<t/t_f<1.0$. It is seen that all three signals (the PSC and the two PSV for the specimens analyzed in previous sections) exhibit a smooth (imperceptible) increasing trend up to specific critical instants, t_c, equal to $(t/t_f)_{PSC}=0.88$, $(t/t_f)_{PSV,34}=0.92$, $(t/t_f)_{PSC,\,140}=0.86$. From these instants on, all three signals start increasing according to a much more rapid manner, and finally, a few seconds before macroscopic fracture the values of all three signals exhibit a sudden drop.

CONCLUDING REMARKS

The electric activity generated in Dionysos marble specimens while they were mechanically loaded was analyzed in terms of the Pressure Stimulated Voltage (PSV) developed. The analysis of the results from two classes of specimens, compressively loaded under load-controlled conditions at two different loading rates revealed that the PSV signals increase very smoothly and almost linearly until a critical time instant, or, equivalently, until a critical stress level. Beyond this critical level, which is designated by the entrance of the specimen into the stage of non-linear response (or, equivalently, into the stage of thermodynamically non-reversible processes), the PSV starts increasing very rapidly, almost until the instant at which the load attains its peak value. A few seconds before the instant of macroscopic fracture, the electric signal recorded by means of the PSV exhibits an abrupt drop.

In parallel, the respective acoustic activity was recorded and analyzed, in juxtaposition to the electric one, both by means of the rate of generation of acoustic signals (in terms of the F-function) and, also, by means of their energy content (in terms of the Cumulative Energy of the Acoustic Emissions). The similarities (from a qualitative point of view) were striking, supporting further the conclusions drawn, also, in a very recent study [26] (from a completely different point of view), that

both these activities (namely, the electric and the acoustic ones), are simply different manifestations of the same damage mechanisms, activated within the bulk of the loaded structure (specimen). The temporal evolution of the PSV was then considered in juxtaposition to that of the Pressure Stimulated Currents (PSC). It was concluded that the two signals exhibit almost identical response (at least from a qualitative point of view), concerning both the early loading levels and, also, load levels approaching the critical ones.

The most important conclusion of the present study is, perhaps, the fact that both activities, namely the acoustic one (quantified either by means of the F-function or by means of the Cumulative Energy of the Acoustic Emissions), and, also, the electric one (quantified either by means of the PSV or by means of the PSC) provide clear signs that can be definitely conceived as pre-failure indices. These signs are the clearly distinguishable abrupt changes of the respective temporal rates of the above parameters. It is worth mentioning here that, for the same class of specimens (i.e., for the same loading rate) these signals are detected within relatively narrow stress levels.

In spite of the narrowness of the interval within which the pre-failure indicators are detected for both techniques employed in this study, it could be concluded (see Fig.8) that for low loading rates the indicator provided by the cumulative energy of the AE precedes that provided by the PSV. This trend seems to be inversed with increasing loading rate. In any case, the small differences detected in this study do not permit definite conclusions about the temporal order of appearance of the pre-failure indicators and, even more, about their reliability and effectiveness. It is obvious that additional experimental data are required, especially in case conclusions are to be drawn about the respective failure mechanisms. Indeed, relative questions, like, for example, whether the earlier increase of the PSV (compared to that of the AE) is due to different underlying failure mechanisms, is difficult to be answered, without a much broader base of experimental data. Archer et al. [6] considered this issue thoroughly, and they, also, appear hesitant to reach categorical conclusions. They made a distinction between two cases, depending on the temporal order of appearance of the respective indicators, and they provide a quite reasonable *hypothesis about the reason that leads to this different order. They state that "… Changes in PSV that occur at the same time or follow AE (and therefore after cracking) may be due to stress redistribution and/or charge redistribution due to formation of new, charged, fracture surfaces. Charge redistribution may be associated with an accumulation of AE events, rather than single events and thus not be instantaneous. The rate of charge redistribution may also be affected by mineralogy and would therefore account for the differences observed between halite and granite". On the other hand, they assume that "… changes in PSV that precede AE (and therefore cracking) may be due to stress accumulation and be occurring at the atomic-scale. This would be consistent with the moving charge dislocation mechanism". However, they, also, avoid drawing definite conclusions mentioning that "… Further investigation is required in order to determine whether this phenomenon is present in other lithology types and whether these observations could be recreated using the same technology in field studies".*

In general, it seems that the imposed loading rate diversifies the results, at least from a quantitative point of view, by "translating" the stress interval within which the pre-failure indices are located: The higher the loading rate imposed the lower the stress level at which the pre-failure indices are detected. Although this issue was not a core target of this study, it was indicated that the role of the loading rate is not negligible, even for the rates considered here, which are close to each other. Again, the need for additional experiments with high dynamic loading schemes, appears to be demanding.

REFERENCES

[1] Grosse, C.U. (2022). Introduction, In: Acoustic Emission testing; Grosse, C.U., Ohtsu, M., Aggelis, D.G., Shiotani, T., eds., Cham, Switzerland Springer Tracts in Civil Engineering, pp. 3–10. DOI: 10.1007/978-3-030-6796-1_2.

[2] Cai, M., Kaiser, P.K., Martin, C.D. (2001). Quantification of rock mass damage in underground excavations from micro-seismic event monitoring, Int. J. Rock Mech. Min. Sci., 38(8), pp. 1135–1145. DOI: 10.1016/S1365-1609(01)00068-5.

[3] Shan, T.C., Li, Z.H., Zhang, X., Niu, Y., Tian, H., Zhang, Q.C., Zang, Z.S., Gu, Z.J., Cai, C., Liu, C. (2022). Infrared radiation and acoustic emission of damage evolution and failure precursory for water-bearing coal, Rock Mech. Rock Eng., 55(12), pp. 7657–7674. DOI: 10.1007/s00603-022-03042-z.

[4] Li, B.L., Wang, E.Y., Li, Z.H., Cao, X., Liu, X.F., Zhang, M. (2023). Automatic recognition of effective and interference signals based on machine learning: A case study of acoustic emission and electromagnetic radiation, Int. J. Rock Mech. Min. Sci., 170, 105505. DOI: 10.1016/j.ijrmms.2023.105505.

[5] Triantis, D., Pasiou, E.D., Stavrakas, I., Kourkoulis, S. K. (2022). Hidden affinities between electric and acoustic activities in brittle materials at near-fracture load levels, Rock Mech. Rock Eng., 55, 1325–1342. DOI: 10.1007/s00603-021-02711-9.

[6] Archer, J.W., Dobbs, M.R., Aydin, A., Reeves, H.J., Prance, R.J. (2016). Measurement and correlation of acoustic emissions and pressure stimulated voltages in rock using an electric potential sensor, Int. J. Rock Mech. Min. Sci., 89, 26–33. DOI: 10.1016/j.ijrmms.2016.08.002.

[7] Vallianatos, F., Tzanis, A. (1998). Electric current generation associated with the deformation rate of a solid: Preseismic and coseismic signals, Phys. Chem. Earth, 23(9-10), pp. 933–938. DOI: 10.1016/S0079-1946(98)00122-0.
[8] Freund, F.T., Kulahci, I.G., Cyr, G., Ling, J.L., Winnick, M., Tregloan-Reed, J., Freund, M.M. (2009). Air ionization at rock surfaces and pre-earthquake signals, J. Atmos. Solar Terr. Phys. 71(17-18), pp. 1824–1834. DOI: 10.1016/j.jastp. 2009.07.013.
[9] Liu, Z., Li, X., Li, Z., Liu, Y., Yang, Y., Feng, J. (2014). Electric potential of the hole wall of concrete under uniaxial compression, J. China Coal Society, 39(Supp.2), pp. 372–377. DOI: 10.13225/j.cnki.jccs.2013.1762.
[10] Kyriazopoulos, A. (2017). Acoustic emissions and electric signal recordings, when cement mortar beams are subjected to three-point bending under various loading protocols, Fracture and Structural Integrity, 11(40), pp. 52–60. DOI: 10.3221/IGF-ESIS.40.05.
[11] Saltas, V., Vallianatos F., Triantis, D., Stavrakas, I. (2018). Complexity in laboratory seismology: From electrical and acoustic emissions to fracture, In: Complexity of Seismic Time Series, Measurement and Application, Chelidge, T., Vallianatos, F., Telesca L. eds., Elsevier, Ch. 8, pp. 239–273. DOI: 10.1016/B978-0-12-813138-1.00008-0.
[12] Li, D., Wang, E., Yue, J., Li, M., Li, L., Wang, D., Liang, W. (2023). Characteristics of pressure stimulated current and damage evolution of granite under progressive uniaxial loading, Sustainability, 15, 14526. DOI: 10.3390/su151914526
[13] Zhang, X., Li, Z., Niu, Y., Cheng, F., Ali, M., Bacha, S. (2019). An experimental study on the precursory characteristics of EP before sandstone failure based on critical slowing down, J. Appl. Geophys., 170, 103818. DOI 0.1016/j.jappgeo. 2019.103818.
[14] Li, M., Wang, H., Wang, D., Shao, Z. (2020). Experimental study on characteristics of surface potential and current induced by stress on coal mine sandstone roof, Eng. Geol., 266, 105468. DOI: 10.1016/j.enggeo.2019.105468.
[15] Li, Z., Shan, T., Wang, E., Niu, Y., Wang, X., Zhang, X., Jia, H., Chen, D., Yin, S., Sun, W. (2024). Experimental study on response and precursor of pressure stimulated currents of combined coal-rock under cycling stress, Int. J. Rock Mech. Min. Sci., 177, 105745. DOI: 10.1016/j.ijrmms.2024.105745.
[16] Mao, W., Wu, L., Xu, Y., Yao, R., Lu, J., Sun, L., Qi, Y. (2022). Pressure-stimulated rock current as loading diorite to failure: Particular variation and holistic mechanisms, J. Geophys. Res.: Solid Earth, 127, e2022JB024931. DOI: 10.1029/ 2022JB024931.
[17] Vallianatos, F., Triantis, D. (2012). Is pressure stimulated current relaxation in amphibolite a case of non-extensivity?, EPL, 99, 18006. DOI 10.1209/0295-5075/99/18006.
[18] Zang, Z., Li, Z., Zhao, E., Kong, X., Niu, Y., & Yin, S. (2023). Electric potential response characteristics and constitutive model of coal under axial static load-dynamic load coupling, Nat. Resour. Res., 32, pp. 2821–2844. DOI: 10.1007/s 11053-023-10261-w.
[19] Shan, T., Li Z., Wang, E., Zhang, X., Jia, H., Wang X., Zhao, E., Niu, Y., Chen, D. (2024). Failure evolution and precursor prediction of fissured sandstone based on power-law behavior of electric potential, Eng. Geol., 346, 107896, DOI: 10.1016/j.enggeo.2024.107896.
[20] Li, D., Wang, E., Feng, X., Wang, D., Zhang, X., Ju, Y. (2023). Weak current induced by coal deformation and fracture and its response to mine seismicity in a deep underground coal mine, Eng. Geol., 315, 107018. DOI: 10.1016/j.enggeo. 2023.107018.
[21] Pasiou, E.D., Triantis, D. (2017). Correlation between the electric and acoustic signals emitted during compression of brittle materials, Fracture and Structural Integrity, 40, pp. 41-51. DOI: 10.3221/IGF-ESIS.40.04.
[22] Zambas, C. (1994). Mechanical properties of Pentelic marbles (in Greek), Publications of the "Committee for the Preservation of the Acropolis Monuments", The "Acropolis Restoration Service", Greek Ministry of Culture, Athens, Greece.
[23] Vardoulakis, I., Kourkoulis, S.K. (1997). Mechanical properties of Dionysos marble, Final Report of the EU Environment Project EV5V-CT93-0300 "Monuments under seismic action", National Technical University of Athens, Athens, Greece.
[24] Kourkoulis, S.K., Exadaktylos, G.E., Vardoulakis, I. (1999). U-notched Dionysos Pentelicon marble in three point bending: the effect of nonlinearity, anisotropy and microstructure, Int. J. Fract., 98, pp. 369–392. DOI: 10.1023/A: 1018614023542.
[25] Stavrakas, I., Kourkoulis, S., & Triantis, D. (2019). Damage evolution in marble under uniaxial compression monitored by Pressure Stimulated Currents and Acoustic Emissions, Fracture and Structural Integrity, 13(50), 573-583. DOI: 10. 3221/IGF-ESIS.50.48.
[26] Triantis, D., Stavrakas, I., Pasiou, E.D., Kourkoulis, S.K. (2025). Cyclic loading of marble: Correlating the attenuation of electric and acoustic activities highlighting criticality indices in terms of Natural Time, Int. J. Min. Sci. Technol., Accepted for publication, Available on-line February 07. DOI: 10.1016/j.ijmst.2024.12.015.

[27] Shan, T., Li, Z., Zhang, X., Jia, H., Wang, X., Wang, E., Niu, Y., Chen, D., Sun, W., Wang, D. (2024). Pressure stimulated current in progressive failure process of combined coal-rock under uniaxial compression: Response and mechanism, Int. J. Min. Sci. Technol., 34(2), pp. 227–243. DOI: 10.1016/j.ijmst.2023.12.008.

[28] Rae, A.S., Kenkmann, T., Padmanabha, V., Poelchau, M.H., Schäfer, F., Dörfler, M.A., Müller, L. (2022). Dynamic compressive strength and fragmentation in sedimentary and metamorphic rocks, Tectonophysics, 824, 229221. DOI: 10.1016/j.tecto.2022.229221.

[29] Vidya Sagar, R., Raghu Prasad, B.K. (2012). A review of recent development in parametric based acoustic emission techniques applied to concrete structures, Nondestruct. Test. Eval. 27(1), pp. 47–68. DOI: 10.1080/10589759.2011. 589029.